On the utilization of radial extrusion to characterize fracture forming limits. Part I – methodology and tooling

Sampaio, Rui F. V.; Pragana, João P. M.; Bragança, Ivo M.F. ; Silva, Carlos M.A. ; Nielsen, Chris V.; Martins, Paulo A.F.

Published in:
Sheet Metal 2023

Link to article, DOI:
10.21741/9781644902417-29

Publication date:
2023

Document Version
Publisher's PDF, also known as Version of record

Materials Research Proceedings **25** (2023) 229-236 https://doi.org/10.21741/9781644902417-29

On the utilization of radial extrusion to characterize fracture forming limits. Part I – methodology and tooling

Rui F.V. Sampaio[1,a], João P.M. Pragana[1,b], Ivo M.F. Bragança[2,c], Carlos M.A. Silva[1,d], Chris V. Nielsen[3,e] and Paulo A.F. Martins[1,f *]

[1]IDMEC, Instituto Superior Técnico, Universidade de Lisboa, Portugal

[2]CIMOSM, Instituto Superior de Engenharia de Lisboa, Instituto Politécnico de Lisboa, Portugal

[3]Department of Civil and Mechanical Engineering, Technical University of Denmark

[a]rui.f.sampaio@tecnico.ulisboa.pt, [b]joao.pragana@tecnico.ulisboa.pt, [c]ibraganca@dem.isel.ipl.pt, [d]carlos.alves.silva@tecnico.ulisboa.pt, [e]cvni@dtu.dk, [f]pmartins.tecnico.ulisboa.pt

Keywords: Forming, Failure, Stress State Transitions

Abstract. This paper and its second part introduce a new formability test based on double-action radial extrusion to characterize material formability in the bulk-to-sheet material flow transitions that are commonly found in metal forming. This first part draws from the presentation of a multidirectional tool, which was designed to convert the vertical press stroke into horizontal movement of the extrusion punches towards each other, to aspects of experimental strain determination, fractography and finite element analysis. The methodology and tooling that are introduced here pave the way for subsequent testing and modelling of the different modes of fracture in three-dimensional to plane-stress evolutions, typical of bulk-to-sheet material flow transitions, by means of the new proposed test.

Introduction

The fracture locus in bulk metal forming is commonly determined by means of upset compression tests performed on cylindrical and tapered specimens and is usually plotted in principal strain space $(\varepsilon_1, \varepsilon_2)$ as a straight line with slope '-1/2' falling from left to right [1]. This line is the graphical representation of the positive and negative strain values that a material withstands at the onset of cracking by out-of-plane shearing, as it was recently proved by Martins et al. [2], and earlier proposed by Kobayashi [3] after observing that vertical and inclined cracks found on the outer surface of these specimens do not run radially.

The proposal of a bilinear fracture locus in principal strain space by Erman et al. [4] resulting from combination of the fracture limit line of slope '-1/2' with a second fracture limit line of slope '-1', is essential to match the strains at failure of the cylindrical and tapered specimens with those of the tensile and upset compression tests performed on rod and cylindrical flanged specimens. This second fracture limit line of slope '-1' corresponds to failure by tension [5] and, in case of cylindrical flanged specimens, the morphology of the cracks is consistent with the experimental observation of vertical cracks running radially at the outer surfaces [6].

Although the bilinear fracture locus is consistent with the experimental results obtained with the different formability test specimens, it gives rise to an 'uncertainty region' (Fig. 1) within which failure occurs by mixed modes resulting from competition between cracking by tension (mode I) and by out-of-plane shearing (mode III). This was recently confirmed by Sampaio et al. [7], who designed a new test specimen to investigate the morphology of the cracks in the 'uncertainty region' of principal strain space and concluded that fracture was triggered by out-of-plane shearing (mode III) and propagate radially by tension (mode I).

Materials Research Proceedings **25** (2023) 229-236 https://doi.org/10.21741/9781644902417-29

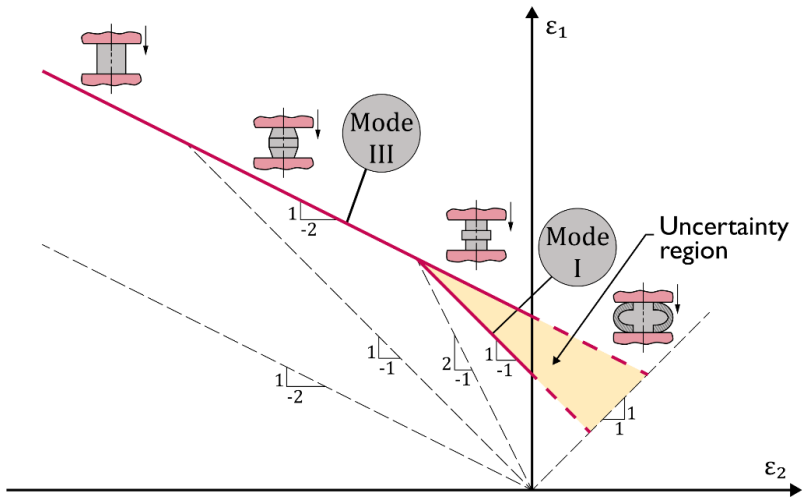

Fig. 1 Bulk formability tests and fracture limit lines in principal strain space.

Transitions from crack opening by mode I to propagation by mode III at the leftmost corner of the 'uncertainty region' were previously observed by the authors during upset compression of cylindrical flanged test specimens made from aluminum AA2030-T4 [8].

In view of the above, Sampaio et al. [7] proposed a new ductile damage criterion based on combination of the Cockcroft and Latham [9] criterion corresponding to crack opening by mode III with a modified version of the McClintock [10] criterion commonly used in crack opening by mode I to model ductile damage over the entire range of stress-triaxiality values, including the 'uncertainty region' of crack opening by mixed modes.

Although research on formability and crack opening modes has been directly, or indirectly, associated with stress triaxiality and, sometimes, also with the Lode parameter [11], there are aspects related to material flow transitions that are not commonly taken into consideration. Accountability of these aspects means, in practical terms, to include the three-dimensional to plane stress material flow transitions (i.e., bulk-to-sheet evolutions) in the list of parameters that are responsible for the competition between the different crack opening modes.

Fig. 2 shows examples of bulk formed parts where plane stress is likely to occur in regions subjected to extensive plastic material flow, (refer to the pink colored regions of the solid rod flange, connecting rod and tube flange, where the final thickness t is much smaller than that of the preforms). The connecting rod is a good example of a well-known occurrence of three-dimensional to plane stress transitions when excess material flows into the flash gutter during impression-die forging.

Under these circumstances, the main objective of this work is to investigate formability in three-dimensional to plane stress material flow transitions by means of a new formability test based on the working principle of double-action radial extrusion [12]. As will be shown, depending on the aspect ratio and overall ductility of the specimens, the diameter-to-thickness ratio of the radially extruded flange may reach typical plane stress values, thereby allowing to analyze strain path evolutions and failure in three-dimensional to plane stress material flow transitions by means of digital image correlation (DIC), scanning electron microscopy (SEM) and finite element modelling.

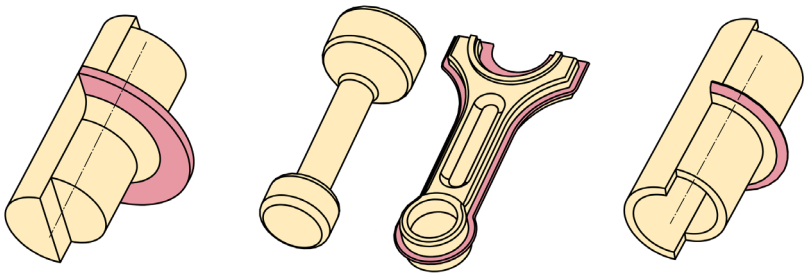

Fig. 2 Schematic representation of bulk forming parts exhibiting regions (refer to the pink color) where material flow takes place under plane stress conditions (solid rod flange, connecting rod and tube flange).

This paper is focused on the multidirectional tool where the double-action radial extrusion setup is installed and, on the methods, and procedures that are used in formability analysis and fractography. Special emphasis is given to a technique for determining the instant of cracking and the corresponding fracture strains by combination of the experimental force vs. time evolutions with the results obtained from digital image correlation.

Numerical simulation with finite elements is also addressed to introduce the fundamentals of exchanging data between two and three-dimensional models at the onset of diffuse necking when asymmetric plastic deformation of the outer flange begins.

Materials and Mechanical Characterization

The experimental work on the new formability test based on double-action radial extrusion made use of a soft aluminum AA1050-O and a medium strength aluminum-magnesium-silicon alloy AA6082 in the annealed (O) and solution heat-treated (T6) state. The materials were supplied in the form of solid rods and the flow curves were determined by means of compression tests carried out on cylindrical test specimens with 20 mm diameter and 20 mm height (Fig. 3).

The compression tests were performed at ambient temperature on an Instron SATEC 1200 kN hydraulic testing machine with a constant crosshead velocity of 5 mm/min. The specimens were lubricated with molybdenum disulphide (MoS2) to ensure near frictionless conditions.

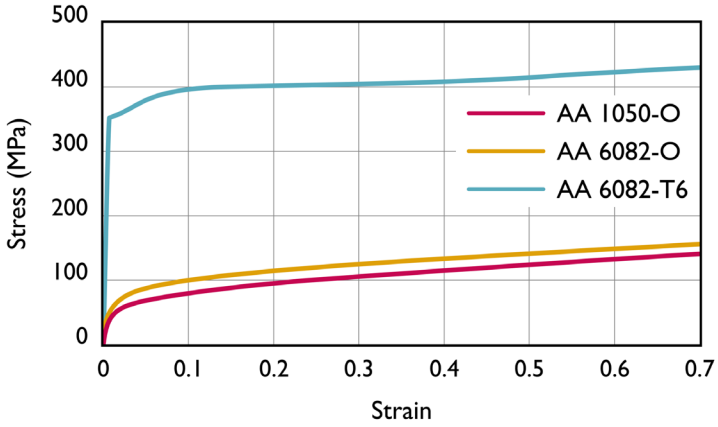

Fig. 3 Flow curves of the aluminum AA1050-O, AA6082-O and AA6082-T6.

Double-Action Radial Extrusion Formability Tests

The double-action radial extrusion formability tests were carried out in a multidirectional tool that was designed and constructed by the authors. The tool allows extruding specimens with different aspect ratios h/d_0 of the free gap height h to the initial diameter d_0 into the volume left between the two dies by compressing the material from two horizontal opposite sides in a single vertical press stroke.

Fig. 4a shows a detail of the tool set in which the movement of the extrusion punches (P) towards each other inside the dies (D) is obtained by means of two cam slide units consisting of a punch holder (H) and a die wedge actuator (A) with a working angle $\alpha = 30°$. Two guided pillars (G) ensure the alignment between the upper and lower tool halves.

The tool set was installed on the hydraulic testing machine that had been previously used to determine the material flow curves.

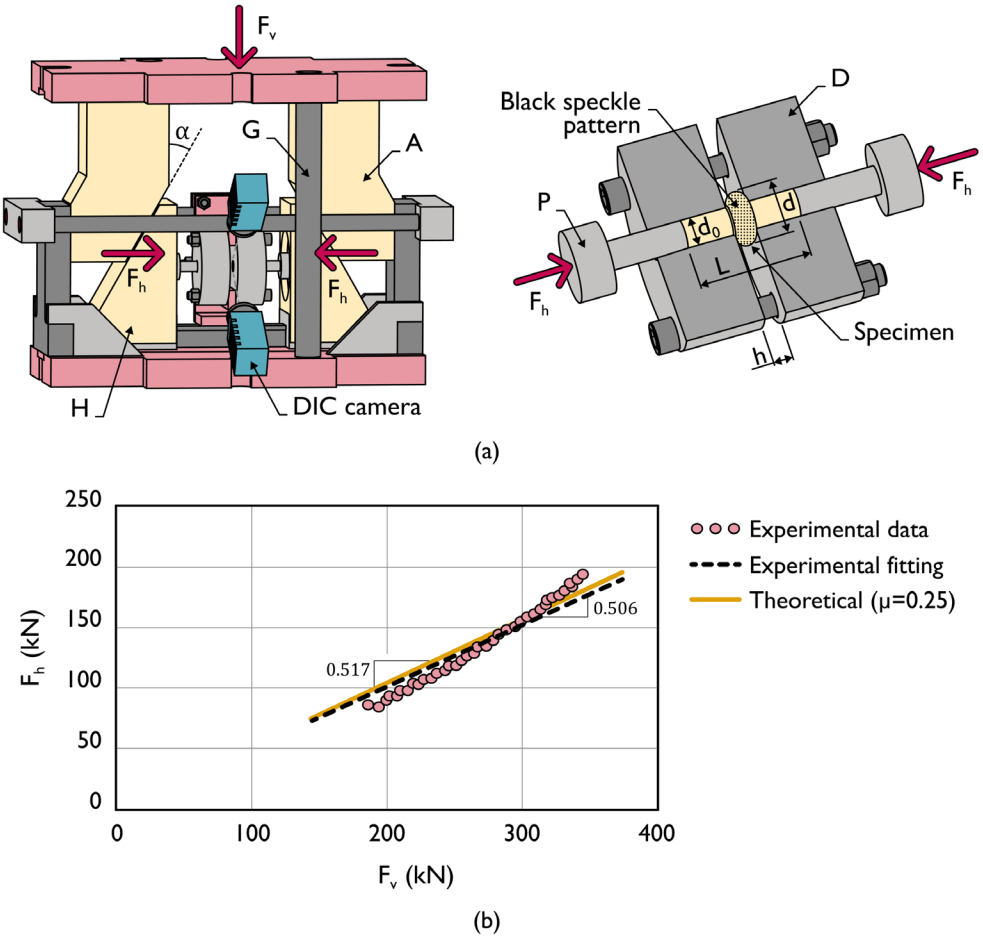

Fig. 4 Double-action radial extrusion formability test. (a) Schematic representation of the tool set with details of the dies and punches, and showing the cameras used by digital image correlation (DIC). (b) Experimental relation between the vertical F_v and horizontal F_h forces.

Force equilibrium across the cam slide units provides the following relation between the horizontal (F_h) and vertical (F_v) tool forces, where μ is the friction coefficient along the contact surfaces,

$$F_h = F_v \frac{\cos\alpha - \mu \sin\alpha}{2(\sin\alpha + \mu\cos\alpha)} = \begin{cases} 0.866\, F_v\,, & \mu = 0 \\ 0.517\, F_v\,, & \mu = 0.25 \end{cases} \quad (1)$$

Compression of cylindrical test specimens made from aluminum AA6082-T6 between straight parallel platens with the double-acting cam slide units and using a single-acting system in which the platens were fixed to the upper and lower bolsters of the tool set, allowed comparing Eq. 1 against experimental data. This is shown in Fig. 4b for $\mu = 0.25$ and the differences at the upper right end are attributed to tool stiffness, elastic deformation, and friction along the surfaces of the cam slide units. For this reason, a slope of 0.506 resulting from the black dashed linear trend line

Materials Research Proceedings **25** (2023) 229-236 https://doi.org/10.21741/9781644902417-29

is used instead of the theoretical estimates with and without friction that are given in Eq. 1 to convert the vertical force F_v measured by the load cell into the horizontal applied force F_h.

Formability Analysis and Fractography

The evolution of the in-plane strains with time $(\varepsilon_1, \varepsilon_2) = f(t)$ on the outer surface of the radially extruded flanges was obtained with a commercial digital image correlation (DIC) system model Q-400 3D from Dantec Dynamics. For this purpose, the initial free gap heigh h of the specimens located in-between the two dies was painted in white and subsequently sprayed with a black speckle pattern (Fig. 4a).

The double-action working principle of the proposed radial extrusion formability test facilitates image acquisition because the measuring window of the DIC system, (equipped with two 6-megapixels resolution cameras with 50.2 focal lenses and f/8 aperture), is fixed and always centered with the vertical symmetry line of the tool set during the entire duration of the test. A frequency of 10 Hz corresponding to 10 images per second was used.

Transformation of the major and minor in-plane strain evolutions with time $(\varepsilon_1, \varepsilon_2) = f(t)$ obtained from DIC into the strain loading paths $\varepsilon_1 = f(\varepsilon_2)$ of principal strain space was carried out by combining and removing the time dependency from the individual evolutions of the major ε_1 and minor ε_2 in-plane strains. The procedure is schematically illustrated in Fig. 5a.

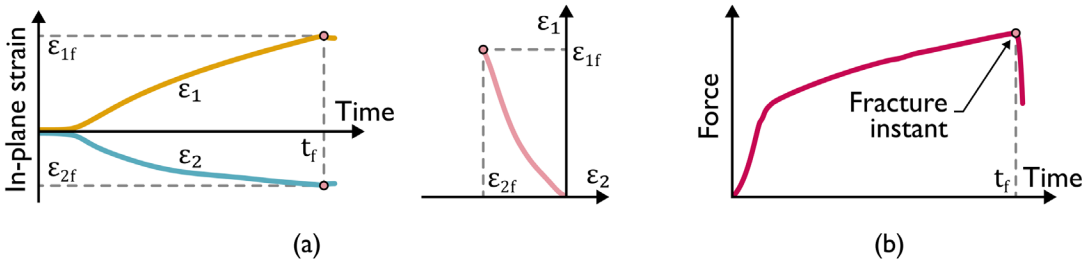

Fig. 5 Methods and procedures involving experimental data in formability analysis. (a) Individual in-plane strain vs. time evolutions determined by digital image correlation (left) and the result of their combination to obtain the strain loading path in principal strain-space (right). (b) Identification of the instant of time at the onset of fracture t_f from the force vs. time evolution.

The instant of time t_f at which cracks are triggered was obtained through identification of the sudden force drop in the experimental evolution of the radial extrusion force with time (Fig. 5b), as earlier proposed by Magrinho et al. [6]. Once t_f is determined, the strains at fracture $(\varepsilon_{1f}, \varepsilon_{2f})$ are easily retrieved from the individual in-plane strain evolutions with time obtained from DIC (Fig. 5a).

After testing, the fractured surfaces were cut out from the specimens for subsequent observation and analysis in a scanning electron microscope (SEM) S2400 from Hitachi. Results are presented in the second part of this paper and provide a correlation between the morphology of the cracks, their opening mechanisms and the corresponding strain loading paths obtained from DIC.

Materials Research Proceedings **25** (2023) 229-236 https://doi.org/10.21741/9781644902417-29

Numerical Simulation

The finite element computer program i-form was utilized to carry out the numerical simulation of the double-action radial extrusion formability test under different operating conditions. The computer program is built upon the finite element flow formulation and was developed by the authors [13] to account for the three major sources of nonlinearity (material nonlinearity, changes of static and kinematic boundary conditions and geometric nonlinearity) that occur in the numerical simulation of metal forming processes.

The numerical simulation strategy utilized by the authors took advantage of the facility that i-form offers to exchange data between two and three-dimensional models because experimental observations revealed that specimens undergo rotationally symmetric plastic deformation conditions up to approximately 30% of the total stroke. Only subsequently, with the occurrence of diffuse necking at the outer flange surface, there is evidence of asymmetric plastic deformation.

Fig. 6 illustrates the overall numerical simulation strategy for a test specimen made from AA1050-O with the different stages carried out by the computer program being illustrated by means of three distinct images:

- Fig. 6a refers to the initial two-dimensional simulation under rotationally symmetric conditions in which the test specimen is modelled as a deformable object and discretized by means of quadrilateral elements. The dies and punches are modelled as rigid objects and discretized by means of linear contact elements with friction,
- Once rotationally symmetric conditions can no longer be utilized, the quadrilateral mesh of the test specimen is automatically rotated counterclockwise about the z-axis to produce a temporary hexahedral mesh like that shown in Fig. 6b. Scalar field variables are rotated accordingly but second-order tensors, like for example the strain tensor ε_{ij}, must be properly transformed as follows,

$$\varepsilon_{ij}^{xyz} = R^T \varepsilon_{ij}^{r\theta z} R \tag{2}$$

In the above equation the superscripts xyz and $r\theta z$ refer to the Cartesian and rotationally symmetric coordinate frames, respectively. The symbol R is the rotation matrix and θ is the angle of rotation shown in Fig. 6,

$$R = \begin{bmatrix} \cos\theta & \sin\theta & 0 \\ -\sin\theta & \cos\theta & 0 \\ 0 & 0 & 1 \end{bmatrix} \tag{3}$$

- The temporary hexahedral mesh contains a significant number of wedge-shaped elements [14] along the z-axis. These irregular elements are automatically eliminated and replaced by regular hexahedral elements with field variables properly transferred between the two meshes (Fig. 6c). The resulting mesh is symmetric along the zx-plane because material was assumed as isotropic. The dies and punches resulting from the rotation of the axisymmetric finite element model continued to be assumed as rigid objects, but their contours were discretized by a mesh of spatial triangles with friction.

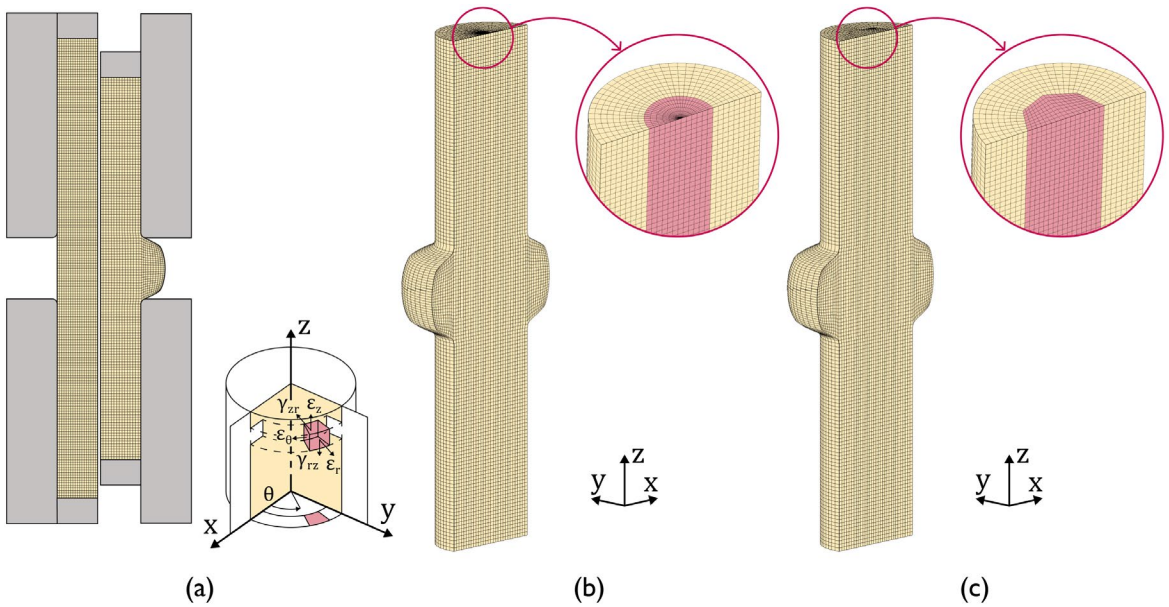

Fig. 6 Methods and procedures utilized in the numerical simulation (AA1050-O with an aspect ratio $h/d_0 = 0.75$). (a) Initial and intermediate rotationally symmetric (2D) meshes, (b) Counterclockwise rotation of the intermediate rotationally symmetric mesh into a temporary three-dimensional hexahedral mesh and (c) Automatic repairment of the temporary three-dimensional hexahedral mesh to obtain a hexahedral mesh without wedge-shaped elements.

The main advantage of the interaction between two and three-dimensional finite element models is the CPU time saving during the first part of the numerical simulation in which specimens undergo rotationally symmetric plastic deformation. In fact, the CPU time between the two and three-dimensional models differs by an order of magnitude of approximately 40 times.

Summary

The methodology and tooling associated with the new proposed double-action radial extrusion test to characterize formability and failure in bulk-to-sheet material evolutions led to the following conclusions:

- The multidirectional tool set allows testing specimens with different aspect ratios h/d_0 of the free gap height h to the initial diameter d_0 into the volume left between the two dies by compressing the material from two horizontal opposite sides in a single press stroke,
- A near-linear correlation can be used to convert the vertical force F_v of the hydraulic testing machine into the horizontal force F_h applied on the extrusion punches,
- Force drops resulting from triggering and subsequent propagation of cracks during the formability tests allow an easy identification of the instant of cracking and of the corresponding fracture strains by combination of the force vs. time evolutions with the in-plane strains obtained from digital image correlation,
- The new test facilitates image acquisition because the measuring window of the DIC system is fixed and always centered with the vertical symmetry line of the tool set during the entire duration of the test,
- Exchange of data between two-dimensional and three-dimensional finite element models at the onset of diffuse necking accounts for significant savings in the overall CPU time because they generally differ by an order of magnitude of approximately 40 times.

Acknowledgements
The authors would like to acknowledge the support provided by Fundação para a Ciência e a Tecnologia of Portugal and IDMEC under LAETA- UIDB/50022/2020 and PTDC/EME-EME/0949/2020.

References

[1] H.A. Kuhn, P.W. Lee, T. Erturk, A Fracture criterion for cold forming, Journal of Engineering Materials and Technology 95 (1973) 213–218. https://doi.org/10.1115/1.3443155

[2] P.A.F. Martins, N. Bay, A.E. Tekkaya, A.G. Atkins, Characterization of fracture loci in metal forming, International Journal of Mechanical Sciences 83 (2014) 112–123. https://doi.org/10.1016/j.ijmecsci.2014.04.003

[3] S. Kobayashi, Deformation characteristics and ductile fracture of 1040 steel in simple upsetting of solid cylinders and rings, Journal of Engineering for Industry 92 (1970) 391–398. https://doi.org/10.1115/1.3427752

[4] E. Erman, H.A. Kuhn, G. Fitzsimons, Novel test specimens for workability testing, in: R. Chait, R. Papirno (Eds.), Compression Testing of Homogeneous Materials and Composites, ASTM International, West Conshohocken, USA, 1983, pp. 279–90. https://doi.org/10.1520/STP36209S

[5] A.G. Atkins, Fracture in forming, Journal of Materials Processing Technology 56 (1996) 609–618. https://doi.org/10.1016/0924-0136(95)01875-1

[6] J.P. Magrinho, M.B. Silva, L.M. Alves, A.G. Atkins, P.A.F. Martins, New methodology for the characterization of failure by fracture in bulk forming, The Journal of Strain Analysis for Engineering Design 53 (2018) 242–247. https://doi.org/10.1177/0309324718758842

[7] R.F.V. Sampaio, J.P.M. Pragana, I.M.F. Bragança, C.M.A. Silva, P.A.F. Martins, Revisiting the fracture forming limits of bulk forming under biaxial tension, International Journal of Damage Mechanics 31 (2022) 882-900. https://doi.org/10.1177/10567895211072580

[8] C.M.A. Silva, L.M. Alves, C.V. Nielsen, A.G. Atkins, P.A.F. Martins, Failure by fracture in bulk forming, Journal of Materials Processing Technology 215 (2015) 287-298. https://doi.org/10.1016/j.jmatprotec.2014.08.023

[9] M.G. Cockroft, D.J. Latham, Ductility and the workability of metals, Journal of the Institute of Metals 96 (1968) 33–9.

[10] F.A. McClintock, A Criterion for ductile fracture by the growth of holes, Journal of Applied Mechanics 35 (1968) 363–371. https://doi.org/10.1115/1.3601204

[11] L. Xue, T. Wierzbicki, Ductile fracture initiation and propagation modeling using damage plasticity theory, Engineering Fracture Mechanics 75 (2018) 3276–3293. https://doi.org/10.1016/j.engfracmech.2007.08.012

[12] R. Balendra, Process mechanics of injection upsetting, International Journal of Machine Tool Design and Research 25 (1985) 63-73. https://doi.org/10.1016/0020-7357(85)90058-7

[13] C.V. Nielsen, P.A.F. Martins Metal Forming: Formability, Simulation, and Tool Design, 1st ed, Academic Press New York, 2021. https://doi.org/10.1016/B978-0-323-85255-5.00006-6

[14] G. Martello, Discretization analysis in FEM models, in: V. Murgul (Ed.) International Scientific Conference Week of Science in SPbPU - Civil Engineering, Saint-Petersburg, Russia. MATEC Web of Conferences 53 (2016) 01063. https://doi.org/10.1051/matecconf/20165301063